DOI: 10.1002/ ((please add manuscript number))
Article type: Full paper

Thin film organic thermoelectric generator based on tetrathiotetracene

Kaspars Pudzs, Aivars Vembris, Martins Rutkis, Simon Woodward*

PhD student K. Pudzs*, Dr. A. Vembris, Dr. M. Rutkis
Institute of Solid State Physics, University of Latvia, 8 Kengaraga Street, Riga LV-1063, Latvia
E-mail: kaspars.pudzs@cfi.lu.lv
Prof. S. Woodward
GSK Carbon Neutral Laboratory for Sustainable Chemistry, University of Nottingham, Jubilee Campus, Nottingham, NG7 2GG, United Kingdom

Keywords: Thermoelectrics, Thin Films, Organic Electronics, Doping.

Thin films of p- and n- type organic semiconductors for thermo-electrical (TE) applications are produced by doping of tetrathiotetracene (TTT). To obtain p-type material TTT is doped with iodine during vacuum deposition of thin films or by post-deposition doping using controlled exposure to iodine vapors. Thermal co-deposition in vacuum of TTT and TCNQ is used to prepare n-type thin films. The attained thin films are characterized by measurements of Seebeck coefficient and electrical conductivity. Seebeck coefficient and conductivity could be varied by altering the doping level. P-type TTT:iodide thin films with a power factor of 0.52 $\mu Wm^{-1}K^{-2}$, electrical conductivity of 130 S m^{-1} and Seebeck coefficient of 63 $\mu V\ K^{-1}$ and n-type TCNQ:TTT films with power factor of 0.33 $\mu Wm^{-1}K^{-2}$, electrical conductivity of 57 S m^{-1} and Seebeck coefficient of -75 $\mu V\ K^{-1}$ are produced. Engineered deposition of both p- and n-type thermoelectric conducting elements on the same substrate is demonstrated. A proof of concept prototype of planar thin film TE generator based on a single p-n couple from the organic materials is built and its power generation characterized.

1. Introduction

Growth in global energy consumption is becoming unsustainable. Improving efficiency in

energy usage has become a global megatrend not only within all industies but across the entirety of society. Minimizing greenhouse gas emissions while simultaneously improving industrial output and competitiveness is a pressing goal. Presently, it is estimated that mankind wastes at least 20% of the 15 terawatts required annually for global power consumption as low level heat (<200 ^{o}C). This amount is larger than the total annual energy usage of all European Union member states. Widespread availability of new low-cost thermoelectric (TE) devices would allow harvesting this energy waste by direct heat-to-electrical energy conversion. TE devices are reliable and compact in comparison to conventional heat engines, because they directly convert thermal to electrical power and vice versa without moving parts or working fluids. Besides this thermoelectric generators (TEGs) have other advantages such as: cleanness, operation without any noise and no discharge of any hazardous substance.[1] Presently the materials used for efficient TE devices are expensive, often not widely available and usually contain unsustainable or toxic elements such as Te, Pb and Se.[2–6] This has stimulated intensive studies seeking new sustainable thermoelectric materials.

The thermoelectric efficiency of a material can be characterized by a dimensionless universal Figure of Merit ($ZT = \sigma S^2 \kappa^{-1} T$), where σ is electrical conductivity, S is Seebeck coefficient, κ is thermal conductivity and T is absolute temperature. TE materials can be divided in groups by appropriate working temperature range. At high temperatures (700-900 K) very promising materials are inorganic clathrates, with ZT near 1, half Heusler alloys with ZT > 0.6 and skutterudites with ZT above 1.[7-12] To achieve high ZT thermal conductivity should be low. Therefore, a general way to improve ZT is to decrease thermal conductivity of the material. Zhao et al. have demonstrated very high ZT > 2 in SnSe single crystals with ultralow thermal conductivity of 0.23 $Wm^{-1}K^{-1}$ at 973 K.[6] A lot of present work is devoted for decreasing thermal conductivity in thermoelectric materials by nanostructuring.[13–15] Unfortunately, the thermoelectrical properties and efficiency of these materials decreases at lower temperatures

(below 200 °C) where the majority of the waste heat reserves abound. There is a pressing need for new TE materials, such as low cost sustainable organic materials, suitable for waste heat harvesting at lower temperature ranges by direct conversion in to electricity.

The TE properties of semiconducting materials can be alternated and optimized by appropriate doping.[16] To ensure maximum performance a balance between electrical conductivity (determined by charge carrier concentration) and Seebeck voltage should be reached. Organic materials are attracting increasing attention for TE applications due numerous advantages including: low thermal conductivity, the possibility to tune their properties via chemical synthesis, low-cost manufacture and sustainable materials abundance.[17–19] Intensive studies of poly(3,4-ethylenedioxythiophene) (PEDOT) and related conductive polymer materials have resulted in high ZT values, reaching up to 0.42.[17,18,20–24] Recently, Cho et al. demonstrated very good TE properties of organic multilayer systems of graphene, carbon nanotubes and conductive polymers, that exceeds classical inorganic TE materials, and reached power factor of 2710 μW $m^{-1}K^{-2}$.[25,26] At same time low molecular weight compounds such as tetrathiofulvalene (TTF), tetracyanoquinodimethane (TCNQ) (see **figure 1**) and metal phthalocyanines have encouraging thermoelectric properties.[27–31] According to theoretical predictions promising TE applications for tetrathiotetracene (TTT) (see figure 1) based materials exist.[32–34] The highest possible electrical conductivity, which is a necessary condition to reach high power factors, should be obtained in single crystals. Unfortunately growing pure and perfect single crystals is a very slow and complicated process, which would hinder the practical applications of particular material. Preparation of thin films is easier, faster and can provide new opportunities, such as flexibility and the possibility to cover varying surface shapes. Previous attention has focused on thin film TEGs prepared from inorganic materials or hybrid materials by combining electro-conductive polymers and TE active inorganic particles.[35–40] Herein we aimed to study the TE properties of TTT based thin films, obtained by thermal evaporation in vacuum, and to demonstrate a practical all organic

TEG. Theoretical calculation shows that by appropriate doping TTT should be viable for both p-type [34] and n-type [33] TE material production. In a previous contribution we have reported our results on the electrical properties and morphology of un-doped TTT thin film.[41] Herein attention was set to optimal doping of TTT the key parameter in reaching the best TEG performance systems.[18,42]

2. Results and Discussion

2.1. P-type semiconductor - TTT Iodide

The simplest way to dope TTT with iodide is a post-deposition process based on sample exposure to the iodine vapor. During such post-deposition doping processes we are able to monitor the electrical conductivity of the TTT thin film by four contact techniques. That allows us to evaluate the doping level of material. As seen in **figure 2**, during exposure to saturated iodine vapors (at atmosphere pressure) the TTT electrical conductivity increased four orders reaching a maximum value within 1 h. Further iodine vapor exposure causes a reduction in TTT thin film conductivity for two reasons. Firstly, the thin film performance is adversely affected by iodine overdoping at the surface, leading the conductivity to one order decrease from 12.3 to 1.5 S m^{-1}. Secondly, the absorption of excessive iodine concentration initiates the start of crack formation within the film. After 1.6 hours, a steep drop in electrical conductivity of more than 3 orders takes place due to thin film disruption through massive crack formation (see figure 2 insets and **figure 3**a).

The cracking is engendered by phase change recrystallization during the intensive iodine doping process due to changes in lattice constants[43] and excessive iodine in thin film. Finally, if the over doped film is exposed to air the electrical conductivity recovers almost one order

of magnitude after the over doped sample is ventilated in air due to desorption of excessive iodine (figure 2: 3.6 to 5 h).

If the exposure to iodine vapors is ended before the conductivity starts to drop down, and chamber vented with ambient air, thin film electrical conductivity typically increases by one order. Apparently excessive iodine desorption as well as more uniform iodine re-distribution within the thin film takes place. Such samples are stable for days, the conductivity remaining close to the value after initial doping. However, if exposure to excess iodine vapor is repeated, then phase change recrystallization is initiated and the conductivity irreversibly decreases.

For optimal electrical conductivity cracking of TTT thin film during doping should be overcome or at least minimized. Iodine diffusion into the thin film is relatively slow therefore an iodine (over) concentration gradient within a film depth easily develops. To avoid this, we applied short cycles of exposure to iodine vapor. The exposure time in for each cycle was 1 minute followed by 30 minutes of equilibration and iodine re-distribution between the doping cycles. In the equilibration period the iodine concentration in the thin film depth is evenly distributed and excessive iodine is avoided thus reducing crack formation. By such post doping methods thin film with conductivities up to 121 S m^{-1} were attained. Although initial increases of iodine doping increase the electrical conductivity the same sample's Seebeck coefficient value decreases from 1170 μV K^{-1} (at conductivity 0.02 S m^{-1}) for pure thin film of TTT to 28 μV K^{-1} at conductivity of 34 S m^{-1} (see **figure 4**). As mentioned above, further doping results in massive recrystallization damage of the thin films. To avoid such crack formation by post deposition doping of pure TTT thin films we attempted a new strategy to p-type TTT:I thin films by iodine co-doping during TTT film deposition. We call this *reactive deposition* by analogy with reactive magnetron sputtering. Through reactive deposition we were able to manipulate the TTT and iodine ratio by changing iodine pressure in chamber during TTT sublimation. In figure 3b the morphology of a TTT:I sample with conductivity of 160 S m^{-1} is shown. The crystallites obtained in such reactive deposition of TTT and iodine

are smaller compared to pure TTT crystals in thin films attained with the same evaporation speed and substrate temperature. The sample was made with TTT evaporation rate of 45 $ng \cdot cm^{-2} \cdot s^{-1}$ and substrate temperature of 23 ^{o}C.

In figure 4 the Seebeck coefficient and power factor dependence on electrical conductivity for reactive deposited samples are shown (hollow vs. solid symbols). Higher iodine doping ratios give minimal improvement in conductivity, which is limited by grain boundaries in the polycrystalline film, but it also drastically reduces the Seebeck coefficient. The low power factor is characteristic of such over doped TTT thin films. In our experiments the highest reached power factor for TTT:I was 0.52 $\mu W m^{-1} K^{-2}$ at the electrical conductivity of 130 S m^{-1} and Seebeck coefficient of 63 $\mu V\ K^{-1}$. At this point exact stoichiometry between TTT and iodine is expected to be TTT_2I_3, which according to literature has the best thermoelectric efficiency.[34,44] The sample was made by reactive deposition but it is similar to samples made by post-deposition iodine TTT doping where 0.46 $\mu W m^{-1} K^{-2}$ and 121 S m^{-1} respectively were realized.

2.2 N-type semiconductor - TCNQ TTT

Thin films of n-type conductivity were produced by TTT and TCNQ reactive co-deposition. Controlled thermal evaporation of TTT and TCNQ from two independent sources was used. Samples with several stoichiometries were prepared by changing the deposition mass ratio of TCNQ/TTT from 0.34 to 10.77 which corresponds to molar ratios of 0.20 to 6.24. The mass ratio was monitored with two quartz crystal microbalances, one for each compound. The TCNQ:TTT molar ratio has a great impact on the thin film morphology, the thin film conductivity and Seebeck coefficient. Higher TCNQ concentrations engenders the formation of flake like crystal morphologies, while in thin films with higher TTT concentration the crystallites are more needle shaped (see **figure 5**).

As it was expected from theoretical calculations the highest power factor is reached at TCNQ and TTT molar ratio ~ 2 (see **figure 6**b).[33] In this case the maximum power factor is 0.33 $\mu Wm^{-1}K^{-2}$, the electrical conductivity 57 S m^{-1} and Seebeck coefficient -75 $\mu V\ K^{-1}$, however the highest Seebeck coefficient -161 $\mu V\ K^{-1}$ is obtained when molar ratio is 3.9. Unfortunately, almost a one order drop in conductivity (6.8 S m^{-1}) takes place at this molar ratio, which results in reduced power factor value -0.18 $\mu Wm^{-1}K^{-2}$.

2.3 Planar Thermoelectric Generator

As mentioned in the introduction a material's Figure of Merit (ZT) is the benchmark for characterization and comparison of thermoelectrics. Unfortunately, reliable measurement of the thermal conductivity of the thin films of our TTT based materials proved untenable preventing ZT calculation. Therefore, to confirm potential practical application of our materials and technology we decided to test their power generation characteristics. First of all, we developed a new concept for a planar single layer thin film TEG device based on tetrathiotetracene (see **figure 7**). Our main goal was to realize very simple TEG preparation, as difficult and expensive fabrication is at odds with the proposed widespread uptake of TEG technology even for efficient devices.

Selection of a fabrication sequence that avoids use of corrosive iodine in the presence of reactive electrodes and n-type material is vital. The optimal, four step, thin film TEG fabrication process is shown schematically in figure 7.

First a p-type "leg" was fabricated in two steps – TTT thin film deposition, followed by TTT doping via exposure to iodine vapor. The post-deposition doping approach was chosen, because it more easily controlled on our current set-up compared to reactive deposition of p-type TTT_2I_3. As a post doping process was used especial care was taken to avoid/minimize film cracking (see above). Thirdly, TTT and TCNQ were co-deposition by thermal

evaporation in vacuum. The conductivity of p-type leg is 88 S m^{-1} and of n-type leg is 12 S m^{-1}, while the Seebeck coefficients are 62 and 118 μV K^{-1} respectively, this results in power factors of 0.33 and 0.16 μW$m^{-1}K^{-2}$. The TEG is completed by 150 nm copper electrode deposition by thermal copper evaporation in vacuum. The current-voltage characteristics of both the p-type and n-type "legs" of the TEG are shown in **figure 8**. A modest temperature gradient of 10 degrees (30 to 40 ºC) was applied by Peltier elements under TEG as our aim is to capture waste heat energy under near ambient conditions. The dimensions of the "legs" in this "proof of concept" device are 2 mm long (direction of ΔT) by 9 mm in width. The total "footprint" of our TEG module is ca. 1 cm^2. The thickness of films or height of "legs" is minimal: 1.2 and 2.5 μm for the p-type and n-type materials respectively. The maximum power of our TEG module at a temperature gradient of 10 ºC reaches 55 pW at 0.9 mV under near ambient conditions. The fabricated TEGs are stable: power generation reduction after two weeks is less than 10%. The generated power is higher than that reported for polyaniline/graphene-PEDOT:PSS bilayer system.[26] We estimate a 10 x 10 cm array of TTT-TEG modules would realize sufficient power for and "internet of things" sensor applications under near ambient conditions. The power of the organic TEG herein is mostly limited by the electrical conductivity of its thin films. The conductivity of such films could be increased by appropriate orientation of crystals. The preferable orientation of the crystallites is along direction of temperature gradient because the conductivity of needle-shaped TTT crystals is anisotropic and aligned with this axis. In addition, grain boundaries as well as orientation are limiting to charge carrier transport. Dense packing and orientation of crystallites parallel to thin film surface should minimize the electron hopping "barriers" and shorten charge transport routes.

3. Conclusion

We have demonstrated that by appropriate doping of (potentially) low cost TTT it is possible to obtain TE active organic thin films of both p- and n-types. We have prepared p-type TTT iodide thin films with power factor of 0.52 $\mu Wm^{-1}K^{-2}$, electrical conductivity of 130 S m^{-1} and Seebeck coefficient of 63 $\mu V\ K^{-1}$ and n-type TCNQ:TTT films with power factor of 0.33 $\mu Wm^{-1}K^{-2}$, electrical conductivity of 57 S m^{-1} and Seebeck coefficient of -75 $\mu V\ K^{-1}$.

This achievement has allowed demonstration of the feasibility of thin film TEG based on organic p-type and n-type materials operating under near ambient conditions. Single couple thin film TEGs were made by deposition of both p- and n-type TTT based materials on one substrate in two separated deposition cycles. Particularly a "proof of concept" single couple TEG of p-type TTT iodide thin films coupled with n-type thin films produced by co-deposition of TTT and TCNQ were prepared The simple fabrication process proposed allows easy duplication of such TEG modules therefore the power of device could be multiplied several times. Power of 5.5 pW K^{-1} was measured for fabricated single couple TEG close to room temperature. This value is mainly limited due to electrical conductivity of polycrystalline thin films. Two options to improve conductivity are proposed: one is optimizing crystallite orientation in thin film plane, another is to reduce the impact of grain boundaries on charge carrier mobility by developing denser packing of polycrystalline thin films. Opportunities to increase thin film electrical conductivity should be pursued to raise the power output of the thin films.

4. Experimental details

Compounds: The TTT (see figure 1) used in experiments was synthesized in the Bulgarian Academy of Sciences by Prof. Dr. V. Dimitrov and co-workers by applying methods described in literature [45]. TTT was purified by thermal gradient sublimation at the University of Wurzburg by the group of Prof. Dr. J. Pflaum. On the basis of ^{1}H NMR spectroscopy [400

MHz, *ca*. 0.3 mM solutions in d_8-toluene, δ_H 7.23 – 7.21 (m, 4H), 6.96 – 6.90 (m, 4H)] and mass spectrometry the initial material was >95% pure and gradient sublimation yielded material with purity >98% TTT. Further enrichment is expected during thin film deposition by thermal evaporation in vacuum. To improve conductivity (p-type), TTT was doped with iodine (Sigma-Aldrich 229695) and to produce n-type material TTT was co-deposited with tetracyanoquinodimethane (TCNQ) (see figure 1). TCNQ was bought from Sigma-Aldrich (157635 Aldrich) and used as received. The purity of substance is 98% and some enrichment can be expected during film deposition as well.

Sample preparation: The designed sample configuration (see **figure 9**) allowed us to perform electrical and thermo-electrical measurements simultaneously. Four gold electrodes placed under thin film were used for in-plane conductivity and Seebeck coefficient measurements.

The substrate was cleaned in turn with deionized water, acetone, chloroform and 2% dilution of Helmanex III detergent in water, more deionized water and finally isopropanol using 15 min cycles in an ultrasonic bath. Afterwards the sample was fixed on a specifically designed sample holder and loaded into the vacuum chamber. Four gold electrodes were deposited by thermal evaporation in vacuum (7×10^{-6} mbar) using shadow masks. The distance between the electrodes and their length was 2 mm and 8 mm, respectively.

Two types of films (p-type TTT:I and n-type TCNQ:TTT) were prepared on glass substrate. TCNQ:TTT thin films were made by co-deposition technique in vacuum. TTT:I thin films were processed by two techniques: reactive TTT doping with iodine during-deposition process or post-deposition doping of the TTT film with iodine. Various ratio TTT:I thin films were deposited by thermal evaporation of TTT under low pressure iodine atmosphere in specially designed system described in experimental setups section. Deposition rates varied from of 20 to 60 $ng \cdot cm^{-2} \cdot s^{-1}$ depending on pressure in chamber and iodine concentration. This deposition rate corresponds to grow rate of around 0.5 nm s^{-1} but it was strongly influenced by the morphology of thin film. The substrate was kept at room temperature (nominally 23 ^oC).

In post-deposition doping techniques TTT thin films were prepared as described by us previously[41] and doped with iodine by holding them in the chamber with saturated iodine vapors in 1 bar pressure. Exposure time determined the doping level within the limits of thin film stability (See results and discussion).

Experimental setups: The equipment for co-deposition consists of a vacuum chamber with two thermal evaporators, two calibrated quartz crystal resonators, two chromel-alumel thermocouples for deposition sources and a sample holder with Peltier element and thermistor for temperature control. Controlled inlet of saturated iodine vapor into the chamber (4×10^{-5} mbar) was ensured through needle valve attached to separated chamber with excess iodine crystals packed into the reactor reservoir under argon. The presence of iodine in the deposition chamber during evaporation allows reactive deposition of TTT:I thin films or post deposition of pre-existing TTT films. To protect the turbo-molecular pump from aggressive iodine vapor a liquid nitrogen trap is installed between chamber and pump system. A quadrupole mass spectrometer Ametek Dycor LC-D is attached to deposition chamber with the aim to monitor composition of the gases. The essential control devices: the TTi QPX600DP power source and the TTi TF960 frequency counter for quartz crystal microbalance readings in our setup are computer moderated (see **figure 10**) to maximize precision during thermal evaporation.

Seebeck coefficient measurements were done by a specialized in house built system. It consists of PTC10 Stanford Research Systems PTC10 Programmable Temperature Controller with two PTC440 TEC drivers and PTC330K 4-channel K-type thermocouple card, Keithley 2182A Digital Low Voltage meter, custom designed sample holder. All measurements were computer controlled and data were acquired using software written in Visual Basic for Excel. Seebeck coefficient measurements in plane were made using sample configuration as shown in **figure 11**.

Temperature differences were measured with two K-type thermocouples which were gently pressed to the thin film at the end of the electrodes.

Each measurement cycle was made by sweeping the temperature gradient across the TEG couple first in one direction, then in the reverse, in a loop such that the midpoint temperature of the thin film in the couple was kept constant at 308 K (35 ^{o}C). In this way both edges of the device both experience a maximum temperature change of $\pm\Delta T$. The Seebeck voltage dependence on temperature was measured by varying the temperature difference (ΔT) in range of ±5 degrees.

Seebeck coefficients were calculated as average from slope coefficients of the obtained relation as shown in **figure 12**. In combination with constant midpoint temperature such looping methods reduce the impact of contact potentials on measurement results. The intercept of linear approximation caused by the contact potential is discarded. An averaged looping procedure also reduces potential errors produced from possible inhomogeneous heating due to thermal contact of the sample and Peltier elements.

Electrical conductivity in the plane of the film was measured by the four probe technique using the four Au electrodes (see above). A Keithley 6487 picoampermeter was used as the current source and voltage measurements were carried out by a Keithley 6514 instrument. Obtained I-V curves exhibit ohmic behavior. Electrical measurements were performed in ambient temperatures (*ca*. 23 ^{o}C).

Thin film morphology was studied by scanning electron microscopy using a TESCAN Lyra 3 FEF-SEM×FIB with a 5 keV electron beam. The conductivity of the studied thin films was high enough to avoid surface charging and therefore additional sputtering of the thin film with a conductive metal layer was not necessary.

The planar organic thin film TEG couple/module was characterized by high precision Keithley 2450 Source Meter Unit. Current-voltage curves were measured both for the single couple TEG and also for each TEG's "leg" separately. Temperature was controlled with the

same PTC10 Stanford Research Systems PTC10 Programmable Temperature Controller used in Seebeck coefficient measurements.

Acknowledgements

This work has been supported by European Commission 7th Framework Programme project (308768) "Waste Heat to Electrical Energy via Sustainable Organic Thermoelectric Devices", National Research Program "Multifunctional Materials and composites, photonics and nanotechnology" (IMIS^2) project "Nanomaterials and nanotechnology". Scientific Research Project for Students and Young Researchers No. SJZ2015/13 realized at the Institute of Solid State Physics, University of Latvia is greatly acknowledged.

Received: ((will be filled in by the editorial staff))
Revised: ((will be filled in by the editorial staff))
Published online: ((will be filled in by the editorial staff))

[1] L. E. Bell, *Science* **2008**, *321*, 1457.

[2] S. Leblanc, *Susmat* **2014**, *1-2*, 26.

[3] H. Beyer, J. Nurnus, H. Bottner, A. Lambrecht, E. Wagner, G. Bauer, *Phys. E* **2002**, *13*, 965.

[4] Z. H. Dughaish, *Phys. B Condens. Matter* **2002**, *322*, 205.

[5] R. J. Korkosz, T. C. Chasapis, S. H. Lo, J. W. Doak, Y. J. Kim, C. I. Wu, E. Hatzikraniotis, T. P. Hogan, D. N. Seidman, C. Wolverton, V. P. Dravid, M. G. Kanatzidis, *J. Am. Chem. Soc.* **2014**, *136*, 3225.

[6] L.-D. Zhao, S.-H. Lo, Y. Zhang, H. Sun, G. Tan, C. Uher, C. Wolverton, V. P. Dravid, M. G. Kanatzidis, *Nature* **2014**, *508*, 373.

[7] V. L. Kuznetsov, L. a. Kuznetsova, a. E. Kaliazin, D. M. Rowe, *J. Appl. Phys.* **2000**, *87*, 7871.

[8] W. Xie, A. Weidenkaff, X. Tang, Q. Zhang, J. Poon, T. Tritt, *Nanomaterials* **2012**, *2*,

379.

[9] Y. W. Chai, T. Oniki, T. Kenjo, Y. Kimura, *J. Alloys Compd.* **2016**, *662*, 566.

[10] M. Gürth, G. Rogl, V. V. Romaka, A. Grytsiv, E. Bauer, P. Rogl, *Acta Mater.* **2016**, *104*, 210.

[11] L. Huang, Q. Zhang, B. Yuan, X. Lai, X. Yan, Z. Ren, *Mater. Res. Bull.* **2016**, *76*, 107.

[12] X. Shi, J. Yang, J. R. Salvador, M. Chi, J. Y. Cho, H. Wang, S. Bai, J. Yang, W. Zhang, L. Chen, *J. Am. Chem. Soc.* **2011**, *133*, 7837.

[13] C. Chang, Y. Xiao, X. Zhang, Y. Pei, F. Li, S. Ma, B. Yuan, Y. Liu, S. Gong, L. D. Zhao, *J. Alloys Compd.* **2016**, *664*, 411.

[14] M. G. Kanatzidis, *Chem. Mater.* **2010**, *22*, 648.

[15] B. Poudel, Q. Hao, Y. Ma, Y. Lan, A. Minnich, B. Yu, X. Yan, D. Wang, A. Muto, D. Vashaee, X. Chen, J. Liu, M. S. Dresselhaus, G. Chen, Z. Ren, *Science (80-.).* **2008**, *320*, 634.

[16] G. J. Snyder, E. S. Toberer, *Nat. Mater.* **2008**, *7*, 105.

[17] O. Bubnova, Z. U. Khan, H. Wang, S. Braun, D. R. Evans, M. Fabretto, P. Hojati-Talemi, D. Dagnelund, J.-B. Arlin, Y. H. Geerts, S. Desbief, D. W. Breiby, J. W. Andreasen, R. Lazzaroni, W. M. Chen, I. Zozoulenko, M. Fahlman, P. J. Murphy, M. Berggren, X. Crispin, *Nat. Mater.* **2013**, *13*, 190.

[18] G.-H. Kim, L. Shao, K. Zhang, K. P. Pipe, *Nat. Mater.* **2013**, *12*, 719.

[19] N. Kim, B. Domercq, S. Yoo, A. Christensen, B. Kippelen, S. Graham, *Appl. Phys. Lett.* **2005**, *87*, 1.

[20] O. Bubnova, X. Crispin, *Energy Environ. Sci.* **2012**, *5*, 9345.

[21] D. Wang, W. Shi, J. Chen, J. Xi, Z. Shuai, *Phys. Chem. Chem. Phys.* **2012**, *14*, 16505.

[22] Y. Du, S. Z. Shen, K. Cai, P. S. Casey, *Prog. Polym. Sci.* **2012**, *37*, 820.

[23] O. Bubnova, Z. U. Khan, A. Malti, S. Braun, M. Fahlman, M. Berggren, X. Crispin, *Nat. Mater.* **2011**, *10*, 429.

[24] Q. Wei, M. Mukaida, K. Kirihara, Y. Naitoh, T. Ishida, *Materials (Basel).* **2015**, *8*, 732.

[25] C. Cho, B. Stevens, J. H. Hsu, R. Bureau, D. A. Hagen, O. Regev, C. Yu, J. C. Grunlan, *Adv. Mater.* **2015**, *27*, 2996.

[26] C. Cho, K. L. Wallace, P. Tzeng, J. H. Hsu, C. Yu, J. C. Grunlan, *Adv. Energy Mater.* **2016**, *6*, 1.

[27] H. Itahara, M. Maesato, R. Asahi, H. Yamochi, G. Saito, *J. Electron. Mater.* **2009**, *38*, 1171.

[28] J. Wüsten, K. Potje-Kamloth, *J. Phys. D. Appl. Phys.* **2008**, *41*, 135113.

[29] Y. Wang, J. Zhou, R. Yang, *J. Phys. Chem. C* **2011**, *115*, 24418.

[30] C. Hamann, *Phys. Status Solidi* **1972**, *10*, 509.

[31] C. Hamann, *Phys. Status Solidi* **1967**, *20*, 481.

[32] A. I. Casian, I. I. Sanduleac, *J. Thermoelectr.* **2013**, *3*, 11.

[33] I. Sanduleac, A. Casian, *J. Electron. Mater.* **2016**, *45*, 1316.

[34] A. Casian, I. Sanduleac, *J. Electron. Mater.* **2014**, *43*, 3740.

[35] P. Fan, Z. H. Zheng, Y. Z. Li, Q. Y. Lin, J. T. Luo, G. X. Liang, X. M. Cai, D. P. Zhang, F. Ye, *Appl. Phys. Lett.* **2015**, *106*, 1.

[36] B. Ju, J.-S. Kim, S.-D. Kwon, S.-J. Yoon, *J. Electron. Mater.* **2009**, *38*, 920.

[37] I. H. Kim, *Mater. Lett.* **2000**, *43*, 221.

[38] R. Venkatasubramanian, E. Siivola, T. Colpitts, B. O'Quinn, *Nature* **2001**, *413*, 597.

[39] P. Fan, Z. Zheng, Z. Cai, T. Chen, P. Liu, X. Cai, D. Zhang, G. Liang, J. Luo, *Appl. Phys. Lett.* **2013**, *102*, 033904.

[40] A. A. A. Rahman, A. Ali Umar, M. H. U. Othman, *Phys. E Low-dimensional Syst. Nanostructures* **2015**, *66*, 293.

[41] K. Pudzs, A. Vembris, J. Busenbergs, M. Rutkis, S. Woodward, *Thin Solid Films* **2015**, *598*, 214.

[42] A. M. Glaudell, J. E. Cochran, S. N. Patel, M. L. Chabinyc, *Adv. Energy Mater.* **2015**,

5, DOI 10.1002/aenm.201401072.

[43] L. C. Isett, *Phys. Rev. B* **1978**, *18*, 439.

[44] V. F. Kaminskii, M. L. Khidekel, R. B. Lyubovskii, I. F. Shchegolev, R. P. Shibaeva, E. B. Yagubskii, A. V. Zvarykina, G. L. Zvereva, *Phys. Status Solidi* **1977**, *44*, 77.

[45] E. A. Perez-Albuerne, *Synthesis of Chalcogenated Polyacenes*, **1973**, (Eastman Kodak Co.), U.S. Patent 3723417 19730327, 4 pp. [Chem. Abs. 78:159696].

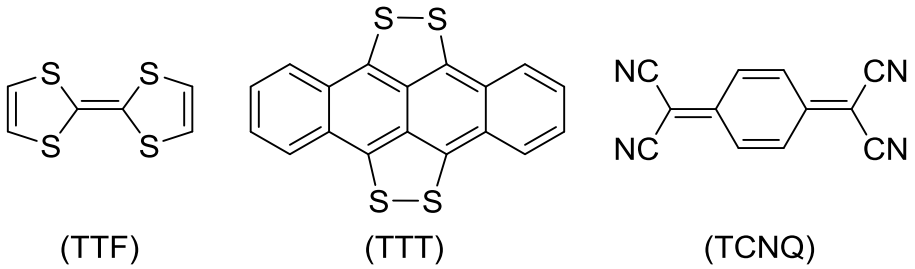

Figure 1. Chemical structures of tetrathiofulvene (TTF), tetrathiotetracene (TTT) and tetracyanoquinodimethane (TCNQ).

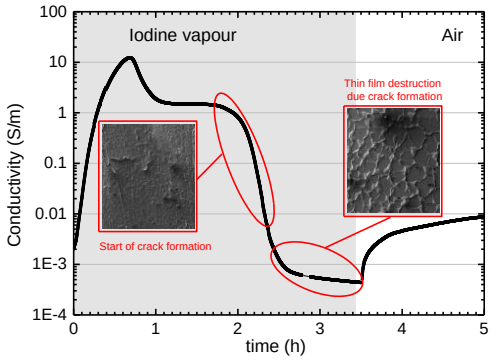

Figure 2. Conductivity changes during TTT thin film exposure to iodine vapors. The insets show SEM images of thin film morphology when crack formation is observed.

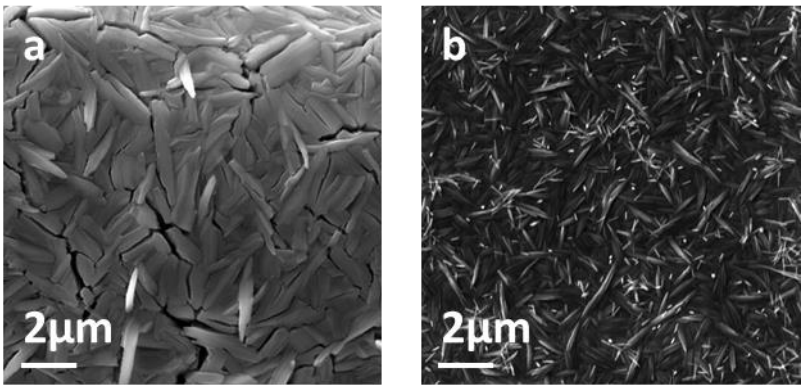

Figure 3. SEM images of TTT iodide thin films. a) Cracks in TTT thin film after over doped with iodine, b) Morphology of the TTT thin film made by reactive deposition of TTT and iodine.

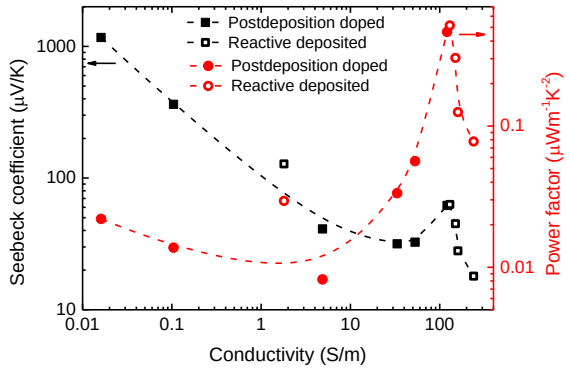

Figure 4. Dependence of Seebeck coefficient and power factor on electrical conductivity of TTT iodide doped thin films for reactive deposited (hollow symbols) and post-deposition doped samples (filled symbols).

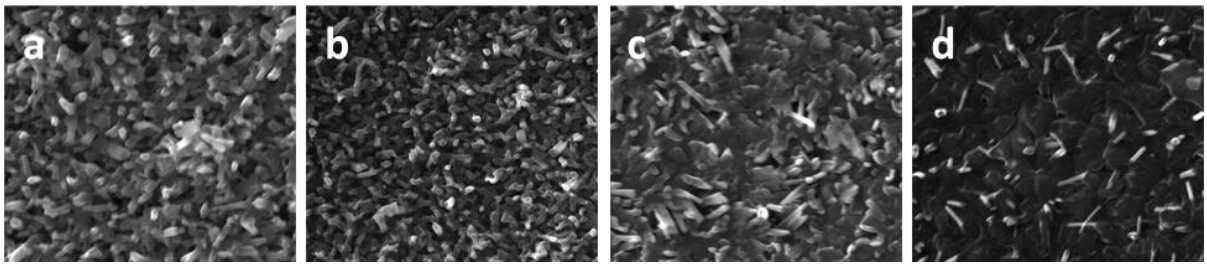

Figure 5. SEM images of TCNQ:TTT thin films with various TCNQ:TTT molar ratio (estimated from mass ratio): a) 1.8, b) 2.6, c) 3.9, d) 18.6.

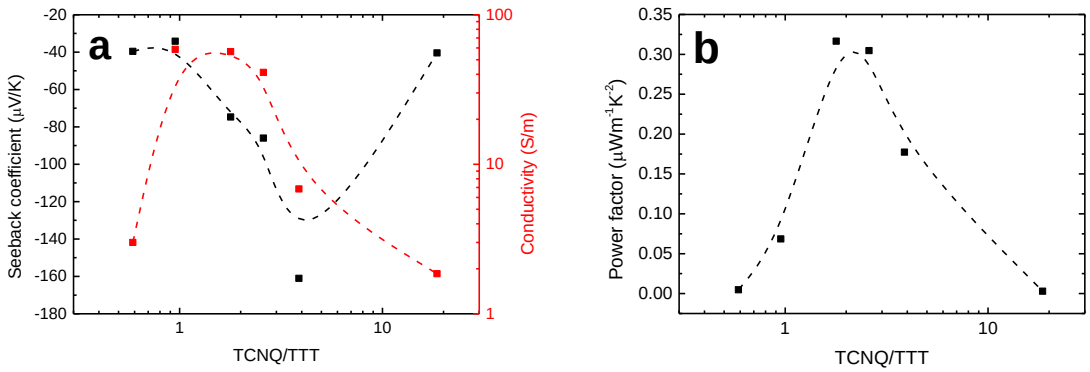

Figure 6. a) Seebeck coefficient, electrical conductivity and b) power factor dependence on TCNQ and TTT molar ratio (estimated from mass ratio).

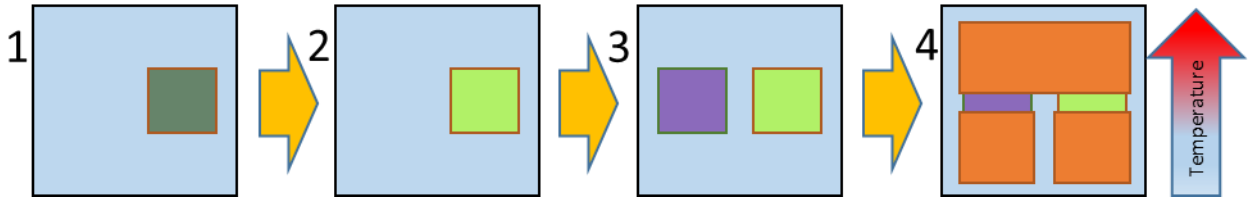

Figure 7. Schematic of thin film TEG fabrication using TTT: 1) TTT deposition, 2) TTT doping with iodine, 3) TTT and TCNQ co-deposition, 4) Cu electrode deposition, the arrow shows the temperature gradient direction.

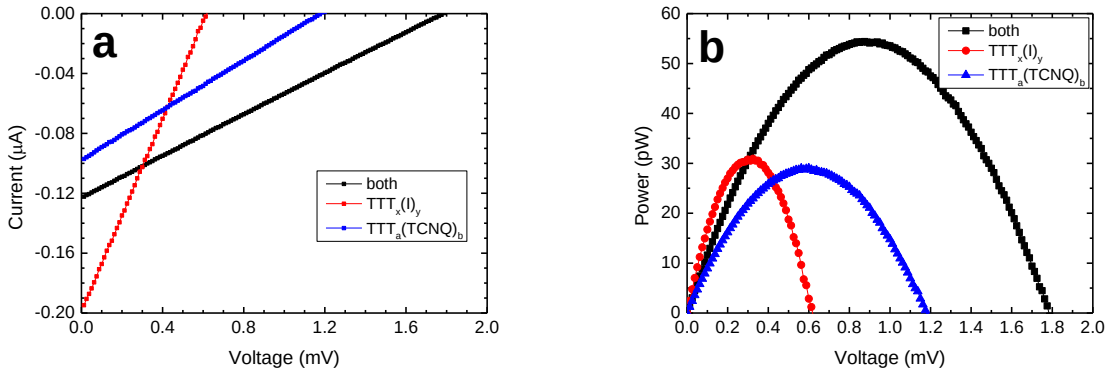

Figure 8. Thermoelectric properties of planar thin film TEG based on TTT. Temperature difference is 10 K. The midpoint temperature is 308 K (35 ^{o}C): a) I-V curves, b) output power of single couple TEG.

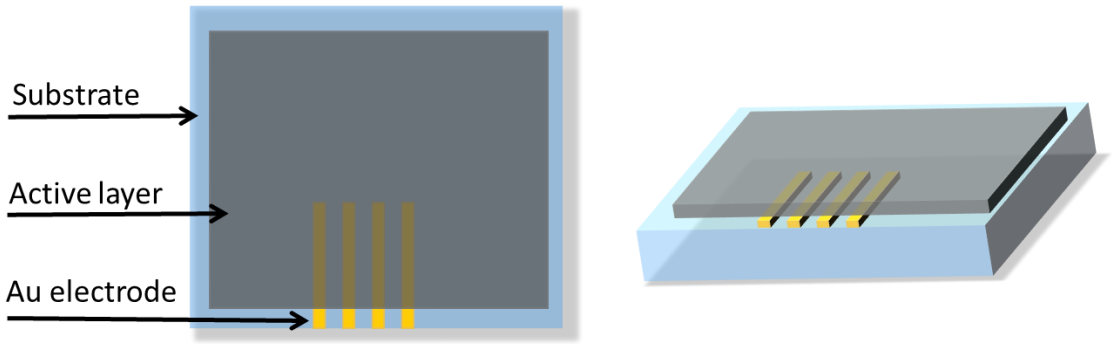

Figure 9. Structure of the samples used for thermo-electric measurements.

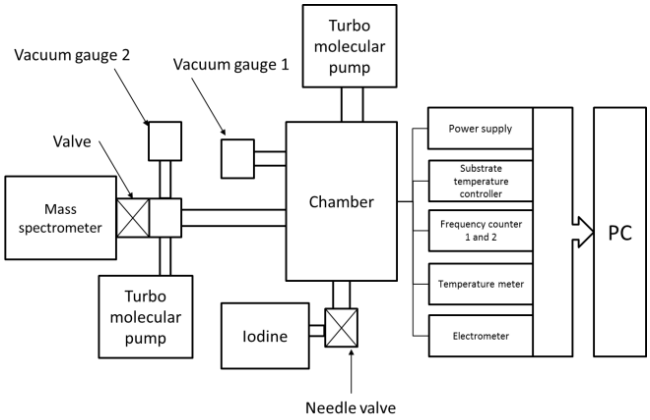

Figure 10. Setup for thermal TTT co-depositions in vacuum.

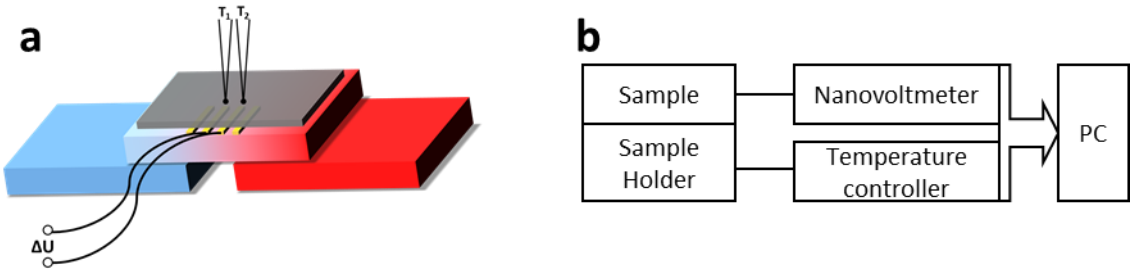

Figure 11. Seebeck coefficient measurement setup: a) schematic representation of sample configuration, b) schematic representation of setup.

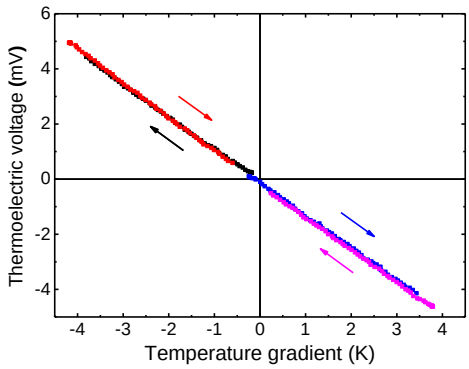

Figure 12. Voltage dependence on temperature difference during Seebeck coefficient measurements for pure TTT thin film sample.

Unique use of a single, simple, organic material tetrathiotetracene (TTT) as a source of both a p and n-type conducting materials types are shown, by forming thin films which are characterized by measurements of Seebeck coefficient and electrical conductivity. Model of p/n thermojunction by vapor printing approaches that potentially could create thousands of junctions within small surface areas are demonstrated.

Thermoelectrics, Thin Films, Organic Electronics, Doping

Kaspars Pudzs*, Aivars Vembris, Martins Rutkis, Simon Woodward

Thin film organic thermoelectric generator based on tetrathiotetracene